Chapter 4
Photofunctional Rare Earth Hybrid Materials Based on Functionalized Microporous Zeolites

Abstract This chapter mainly focuses on recent research progress in photofunctional rare earth hybrid materials based on functionalized microporous zeolites. It covers photofunctional rare earth hybrid materials based on zeolite X, zeolite A, and zeolite L, respectively. Among them the emphasis is put on the hybrid systems based on zeolite L because they are most intensively studied.

Keywords Rare earth ion • Photofunctional hybrid material • Functionalized zeolite • Luminescence

4.1 Zeolite, Rare Earth Ion-Functionalized Zeolites, and Their Photophysical Properties

Molecular sieves are microporous solids with pores of the size of molecular or nanoscale dimensions, 0.3–2.0 nm in diameter. Some are crystalline with a uniform pore size delineated by their crystal structure, for example, zeolites. Most molecular sieves in practice today are zeolites [1].

Zeolites are natural or synthetic crystalline aluminum silicate of group IA and group IIA elements, such as sodium (Na), potassium (K), magnesium (Mg), and calcium (Ca), whose pores are of molecular dimensions [2]. Chemically, they are represented by the empirical formula: $M_{2n}O{\cdot}Al_2O_3{\cdot}ySiO_2{\cdot}wH_2O$ where y is 2–200, n is the cation valence, and w represents the water contained in the voids of the zeolite. Structurally, they are complex crystalline inorganic polymers based on an infinitely extending three-dimensional, four-connected framework of AlO_4 and SiO_4 tetrahedra linked to each other by the sharing of oxygen ions. Each AlO_4 tetrahedron in the framework bears a net negative charge which is balanced by an extra-framework cation. The framework structure contains intracrystalline channels or interconnected voids that are occupied by the cations and water molecules. The cations are mobile and ordinarily undergo ion exchange. The water may be removed reversibly, generally by the application of heat, which leaves intact a crystalline host structure permeated by the micropores and voids which may amount to 50% of the crystals by volume. The intracrystalline channels or voids can be one-, two-, or three-dimensional. The preferred type has two or three dimensions to facilitate

B. Yan, *Photofunctional Rare Earth Hybrid Materials*,
Springer Series in Materials Science 251, DOI 10.1007/978-981-10-2957-8_4

intracrystalline diffusion in widespread application such as catalysis, gas absorption, water filtration, etc. [1, 2]. The structures of zeolite comprise of a three-directional network of $[AlO_4]^{5-}$, and $[SiO_4]^{4-}$ tetrahedron linked via bridging oxygen atoms are assembled into secondary building units which may be simple polyhedra, such as cubes, hexagonal prisms, or cubo-octahedra. The secondary units in the final framework structure generate different kinds of holes of negative charge density due to the presence of Al^{3+}, and the net negative charge can be balanced by metallic cations, protons, or cationic complex. Cages and channels of discrete size in the zeolite are normally occupied by water molecules [1, 3].

More than 70 novel, distinct framework structures of zeolites are known, which exhibit pore sizes from 0.3 to 1.0 nm and pore volumes from about 0.10 to 0.35 cm^3/g. Typical zeolite pore sizes include small-pore zeolites with 8-ring pores, free diameters of 0.30–0.45 nm (e.g., zeolite A); medium-pore zeolites with 10-ring pores, 0.45–0.60 nm in free diameter (ZSM-5); large-pore zeolites with 12-ring pores of 0.6–0.8 nm (e.g., zeolites X, Y); and extra-large-pore zeolites with 14-ring pores (e.g., UTD-1), respectively. Some important types of zeolite have been used in commercial applications, including the zeolite minerals mordenite, chabazite, erionite, clinoptilolite, and the synthetic zeolite types A, X, Y, and L [1, 2]. The low silica zeolites represented by zeolites A and X are aluminum-saturated, have the highest cation concentration, and give optimum adsorption properties in terms of capacity, pore size, and three-dimensional channel systems. They represent highly heterogeneous surfaces with a strongly hydrophilic surface selectivity. The intermediate Si/Al zeolites (Si/Al of 2–5) consist of the natural zeolites erionite, chabazite, clinoptilolite, and mordenite and the synthetic zeolites Y, mordenite, omega, and L. These materials are still hydrophilic in this Si/Al range. The high silica zeolites with Si/Al of 10–100 can be generated by either thermochemical framework modification of hydrophilic zeolites or by direct synthesis. In the modification route stabilized, siliceous variants of Y, mordenite, and erionite and over a half-dozen other zeolites have been prepared by steaming and acid extraction. These materials are reported to be hydrophobic and organophilic and represent a range of pore sizes from 0.4 to 0.8 nm.

Zeolites are endowed with uniform cavities and channels, which have opened new possibilities for numerous application fields, not only in catalysis and absorption but also for the utility of host materials for photoluminescence center. One of the earliest applications of zeolite photoluminescence is to probe coordination environments of ions [4]. Among all the paths used to functionalize zeolite, ion exchange method should be the most popular one. Because zeolite has many cages and channels, cations are free to migrate in and out zeolite structures. The luminescence properties of rare earth ion-exchanged zeolite are exploited to probe microenvironment of zeolite [5–7]. Rare earth ions have large ion size so that a hydrated ion cannot migrate from a supercage to a small sodalite to replace the residing Na^+ ions. The ion exchange saturated level of La-NaY is 0.69 ± 0.01 at 25 °C. Rare earth ions can only replace Na^+ ions in the supercage unless the temperature of exchange is raised much more higher. Higher temperature of treatment facilitates rare earth ions going into the sodalite cages and double hexagonal prisms [8, 9]. Luminescence

spectra are usually used to track the transfer of energy on solid surface from absorber to an emitter, and lifetime experiments are used to obtain the number of coordinated water molecules [10].

Chen et al. investigate the photoluminescence and photostimulated luminescence of Tb^{3+} and Eu^{3+} co-doped in zeolite Y [11]. The luminescence from the hydrated zeolite containing Tb^{3+} and Eu^{3+} prepared at room temperature is very weak due to the dissipation of excitation energy by OH vibrations. However, the luminescence is enhanced greatly when the sample is treated at 800 °C, which is due to the loss of water and the migration of the ions from the supercages to the sodalite cages. Strong photostimulated luminescences of both Tb^{3+} and Eu^{3+} are firstly detected in the sample prepared at 800 °C. The photostimulated luminescence of Tb^{3+} is due to the recombination of electrons with Tb^{4+} ions, while the photostimulated luminescence of Eu^{3+} is caused by energy transfer from Tb^{3+} to $Eu^{3.+}$ The existence of Tb^{4+} and Eu^{2+} ions confirmed by EPR measurements is due to charge transfer from Tb^{3+} to $Eu^{3.+}$ The occurrence of photostimulated luminescence and discrete emission lines in blue (434 nm), green (543 nm), and red (611 nm) colors indicate that this material has potential applications in white light-emitting devices and erasable optical storage. The photoluminescence intensity of Eu^{3+} is higher than the photoluminescence intensity of Tb^{3+}, but it is contrary to their photostimulated luminescence intensity.

Jüstel et al. study the optical properties of Tb^{3+}/Ce^{3+}-doped zeolites in the UV and green spectral emission range, with an emphasis on ultraviolet (UV) and vacuum ultraviolet (VUV) excitation and luminescence [12]. Ce^{3+}-sensitized Tb^{3+} green emission possesses a quantum yield of 85% under 330 nm excitation, which is from an efficient $Ce^{3+} \rightarrow Tb^{3+}$ energy transfer. Unfortunately, low absorptivity at 254 nm due to low Ce^{3+} concentrations or low Tb^{3+}/Ce^{3+} ratios restricts their applicability as phosphors for Hg-based discharges such as in conventional fluorescent lamps. Near band edge excitation at 172 nm reveals an immediate quantum yield of 50% enabled by a zeolite $\rightarrow Ce^{3+}(5d^1) \rightarrow Tb^{3+}(4f^75d^1)$ energy transfer channel, which may be exploited for the down-conversion of the Xe_2 excimer emission. In VUV investigations the optical bandgap of zeolite X is located at 6.9 eV. The introduction of Ce^{3+} into Tb-X zeolites results in a remarkable increase of the green quantum yields upon near band edge excitation, which is due to the Ce^{3+} d-states in resonance to the optically generated excitons in the zeolite. The capability of the zeolite host lattice to transfer excitation energy into sensitizer or rare earth ion levels may be of immediate interest in applications such as Xe_2* excimer discharge-driven lighting systems.

Zeolite L (ZL) is a cylindrically shaped, porous aluminosilicate having a one-dimensional channel system oriented along the c-axis. Mech et al. show how the intentionally generated oxygen vacancies can be used to indirectly excite the Er^{3+} ions loaded in ZL and generate the 1.54 μm emission [13]. The PL is effectively produced by a photoinduced energy transfer from the oxygen vacancies, which act as a light-harvesting antenna and can be excited in a very broad spectral range (from 355 nm to 700 nm in the whole UV and visible region) with common light sources to the rare earth ion. The role of the vacancies is clearly evidenced by the decay time of the obtained NIR emission, which results to be three times longer than that mea-

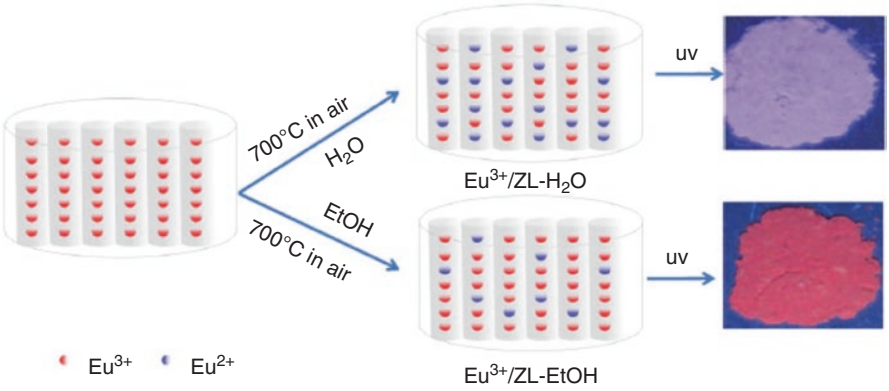

Fig. 4.1 Schematic of the preparation procedure and digital photo of samples irradiated under UV light (Reprinted with permission from Ref. [14]. Copyright 2012 the Royal Society of Chemistry)

sured in the same dehydrated host without oxygen defects. So it is possible to obtain sensitization of the Er^{3+} NIR emission, using white light excitation, by incorporation of Er^{3+} into the ZL structure, whereby oxygen vacancies have been created.

Li et al. have found that annealing of Eu^{3+}-functionalized ZL (Eu^{3+}/ZL) at 400 to 800 °C can produce a strong and bright violet-blue emission, [14] whose real origin of the emission is still not clear and needs to be identified. They confirm the reduction of Eu^{3+} to Eu^{2+} in the annealed Eu^{3+}/ZL crystals during the annealing process at 700 °C under an air atmosphere, and both Eu^{3+} and Eu^{2+} ions are present in the annealed Eu^{3+}/ZL crystals. Washing Eu^{3+}/ZL crystals with water followed by annealing can give them a strong violet–blue luminescence, while ethanol can give them bright red luminescence, which results from the strong quenching of Eu^{3+} luminescence in the water-washed samples (Fig. 4.1). So zeolite crystals can be used as an ideal host to obtain Eu^{2+} ions that can emit from the UV region to the red region depending on the symmetry and crystal field strength around Eu^{2+}.

They further study the red emission and NIR emission from a RE^{3+}- and Bi^{3+}-cofunctionalized ZL (RE^{3+}/Bi^{3+}-ZL, RE = Eu, Nd) by a simple ion exchange process and subsequent annealing. The morphology and size distribution of the RE^{3+}/Bi^{3+}-ZL remain almost unchanged during the synthesis process as revealed by SEM images and can easily be tuned by an appropriate choice of ZL crystals (Fig. 4.2) [15]. It is interesting that Eu^{3+} in the Eu^{3+}/Bi^{3+}-ZL has a lifetime of 1.93 ms and a $^5D_0$ quantum efficiency of 67%, which is suitable for cooperation with UV-emitting LEDs because of its ability of near UV excitation. Nd^{3+} in the annealed Nd^{3+}/Bi^{3+}-ZL also attains in a lifetime of 0.196 ms, which may make it a potential candidate for generating laser emission at 1060 nm for optical device application.

Duan et al. synthesize a great diversity of ion-exchanged zeolite Y processing high ion-exchanged capability and numerous hospitable cavities and sites. As for zeolite modified with Y^{3+} or Zn^{2+}, investigations of doping monometal ions and bimetal ions are carried out to enrich the theoretical knowledge of the photoluminescence of ion-exchanged zeolite Y [16]. The metal ion-exchanged zeo-

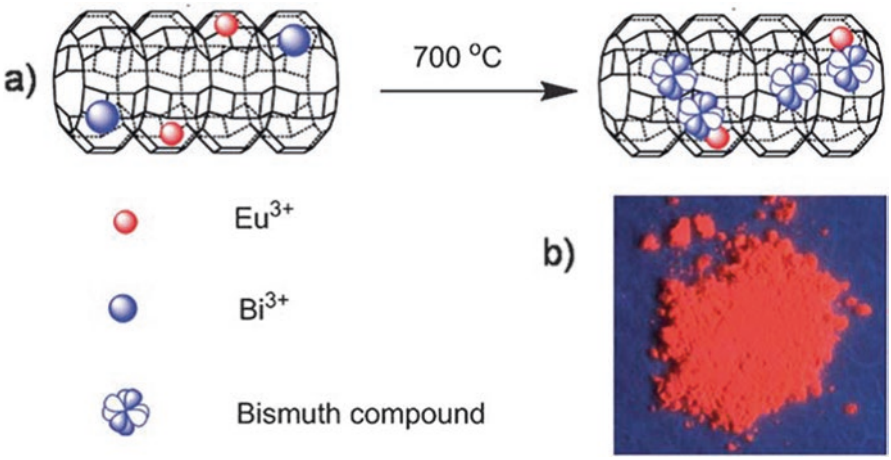

Fig. 4.2 The scheme for (*a*) synthetic strategy pursued to obtain luminescent materials; (*b*) digital photo of Eu^{3+}/Bi^{3+}-ZL under UV irradiation (365 nm). Reprinted with permission from Ref. [15]. Copyright 2011, the Royal Society of Chemistry

lites are conveniently prepared through suspending zeolite into certain nitrate aqueous solution (Fig. 4.3 (top)). Most of them are octahedral NaY zeolite nanocrystals with a small amount of gmelinite as impurity (SEM image in Fig. 4.3 (bottom)), which have a regular and uniform structure with the diameter of about 250 nm. The morphology of zeolite NaY crystals and their size are largely dependent on the preparation conditions such as temperature, time, and the composition and molar ratio of the starting gels. The time-dependent experiment is carried out to study the morphology transformation of zeolite. When prolonging synthesis time, the morphology of zeolite transforms from zeolite NaY to gmelinite. When ion exchange is performed at low temperature and low pressure, the exchanged ions are located in the β supercage of NaY zeolite, which includes (1,1,1) crystal plane, since it is the maximum ion exchange window of NaY zeolite. The intensity of (1,1,1) crystal plane of rare earth ion-exchanged zeolite is relatively low than that of transition metal ion-exchanged zeolite, mainly because the ion radius of rare earth is much larger than that of transition metal ion, which leads to partly inevitable damage on (1,1,1) plane. The emission in EuNaY following laser excitation at 394 nm contains the $^5D_0 \rightarrow {}^7F_J$ (J = 0, 1, 2, 3, 4) transition at 579, 590, 614, 653, and 698 nm and also includes $^5D_5 \rightarrow {}^7F_J$ transition (J = 0, 1, 2) at 524, 535, and 555 nm, together with a broadband around 478 nm due to the emission of excited zeolite structure. The Ce^{3+} emission in CeNaY zeolite shows a broadband at 350 nm due to the transition of 5d → $^2F_{5/2}$ and 5d → $^2F_{7/2}$ ground states. Tb^{3+} emission in TbNaY contains the $^5D_4 \rightarrow {}^7F_J$ (J = 3, 4, 5, 6) transition at about 621, 583, 545, and 489 nm as well as the broadband around 437 nm due to the emission of excited zeolite structure. The emission spectra of rare earth ion-exchanged zeolites reveal that the characteristic rare earth emission peaks are generated by its nature 4f (or 5d) energy level

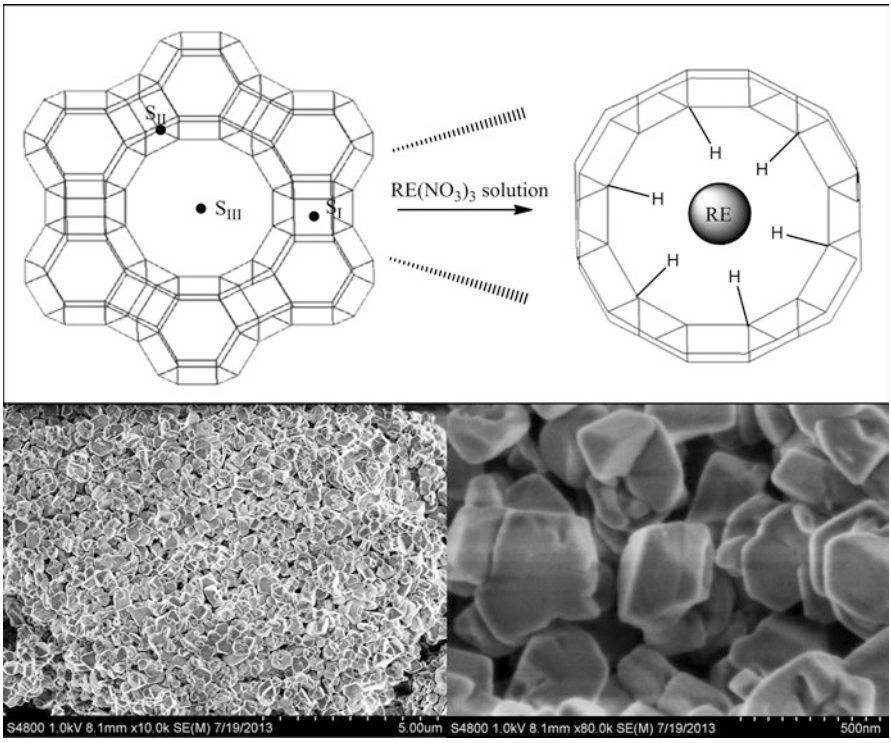

Fig. 4.3 (*Top*) The scheme for synthesis of the rare earth ion-exchanged zeolite: ion exchange process to introduce rare earth ions into NaY zeolite under the condition of 373 K. The rare earth ions are mainly on the S_{III} site because of relatively low heating treatment temperature. (*Bottom*) Selected SEM images of synthesis NaY zeolite (Reprinted with permission from Ref. [16]. Copyright 2014 Wiley Publisher)

transition, but not by the excitation band of zeolite. It's remarkable that EuNaY exhibits white light which shows strong applied value in luminescent devices.

4.2 Photofunctional Rare Earth Hybrid Materials Based on Functionalized Zeolite-FAU

To get some novel materials, it is advantageous to introduce substance of interest by ion exchange, vapor impregnation, solid-state diffusion, or ship-in-bottle synthesis. Herein the photofunctional rare earth hybrids based on functionalized zeolite faujasite type (FAU, including Y type) are firstly introduced.

Wada et al. succeed in drastically enhancing the near-infrared (NIR) emission of Nd^{3+} by ligating it with bis(perfluoromethylsulfonyl)amine in cages of a nanocrystalline, large-pore zeolite FAU (Fig. 4.4) [17]. The octahedral shape of each particle

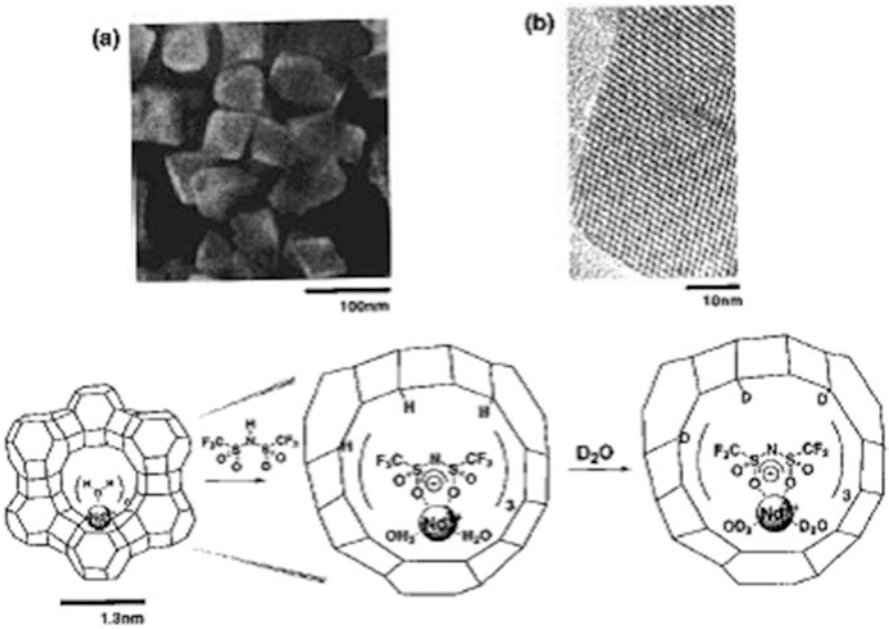

Fig. 4.4 FE-SEM (*a*) and TEM (*b*) views of the nanosized zeolite FAU prepared. The scheme displayed below the photos shows the conceptual process of the ship-in-bottle synthesis and the treatment with D_2O (Reprinted with permission from Ref. [17]. Copyright 2000 American Chemical Society)

and the fine structure of the zeolite cage are shown in Figure 4.5a and b, respectively. The particle sizes of the crystallites are 50–80 nm. The Nd-exchanged n-FAU powder is confirmed to have the composition of Si/Al = 2.8 and the exchange degree of (Na^+ by Nd^{3+}) 85–95%. After being degassed and kept in contact with vapor of bis(perfluoromethylsulfonyl)amine (PMS-H), the final hybrid (Nd(PMS)-n-FAU) is prepared, whose differential scanning calorimetry analysis shows an endothermic peak above the decomposition temperature of the neodymium with PMS and supports the formation of the complex inside the cages. The quantum yield for the emission of Nd(PMS)-n-FAU is determined to be $(9.5 \pm 1.0) \times 10^{-2}$ under excitation at 585 nm, being the highest value ever observed for Nd^{3+} emission in organic media. Nd-(PMS)-n-FAU particles aggregate to some extent with particle size distribution ranging from 100 to 175 nm. The strong emission for the hybrid system should be attributed to suppression of the relaxation of the excitation energy of Nd^{3+} through the vibrational excitation by the low-vibrational zeolite cage wall and the energy migration at collisions by locating Nd^{3+} separately in the cages. Furthermore, ligation of the emitting Nd^{3+} center with PMS in the zeolite cages should play an important role in retarding the vibration excitation caused by -OD groups surrounding the emitting centers.

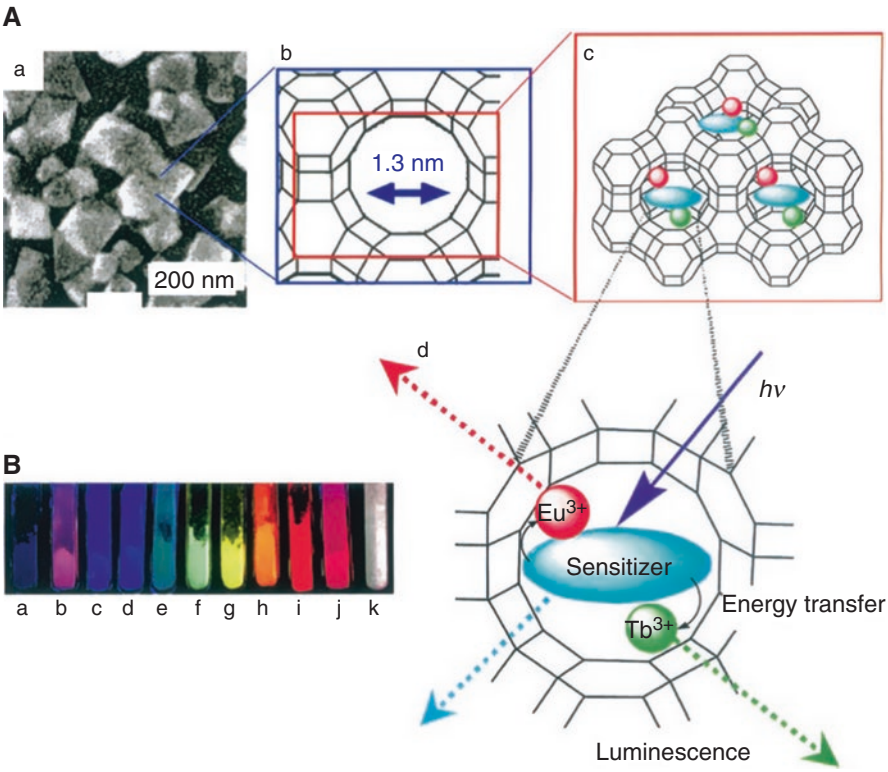

Fig. 4.5 (**a**) (*a*) SEM image of faujasite zeolite; (*b*, *c*) views of the framework structure of the ZX crystal; the sizes of the 12-ring open window and inner cage are 0.7 and 1.3 nm, respectively; (*d*) luminescence from the sensitizer molecule and emission of Tb^{3+} and Eu^{3+} ions through energy transfer from the sensitizer molecule. (**b**) Photographs of the photoluminescence from ZX samples, with colors varying from violet to red depending on the incorporated amounts of Tb^{3+} and Eu^{3+} ions, the type of photosensitizer (bzp or acbp), and the excitation wavelength (Reprinted with permission from Ref. [18]. Copyright 2006 Wiley)

They further investigate the rare earth ion-exchanged zeolites FAU incorporated with a photosensitizer (Figure 4.5A) that exhibit successful RGB photoluminescence depending on which rare earth ions and photosensitizers are used (Figure 4.5B) [18]. The color can also be finely tuned by varying the temperature and the excitation wavelength. The RE^{3+}-exchanged zeolite X is degassed for dehydration and is then either exposed to benzophenone (bzp) vapor or stirred in a solution of 4-acetylbiphenyl (acbp) in ethanol at room temperature. The reaction sequence is carried out on a vacuum line to avoid exposure of the zeolites to the atmosphere. The colors obtained varied from violet (b) to red (j) through blue (c, d) and green (e) by changing the amounts of the RE^{3+} and the nature of the sensitizer (bzp or acbp) (Figure 4.5B). The encapsulation of acbp in the zeolite cavity gives rise to blue emission besides the red and green colors emitted by Eu^{3+} and Tb^{3+} ions, respectively, leading to simultaneous RGB photoluminescence, while it is contrary to bzp.

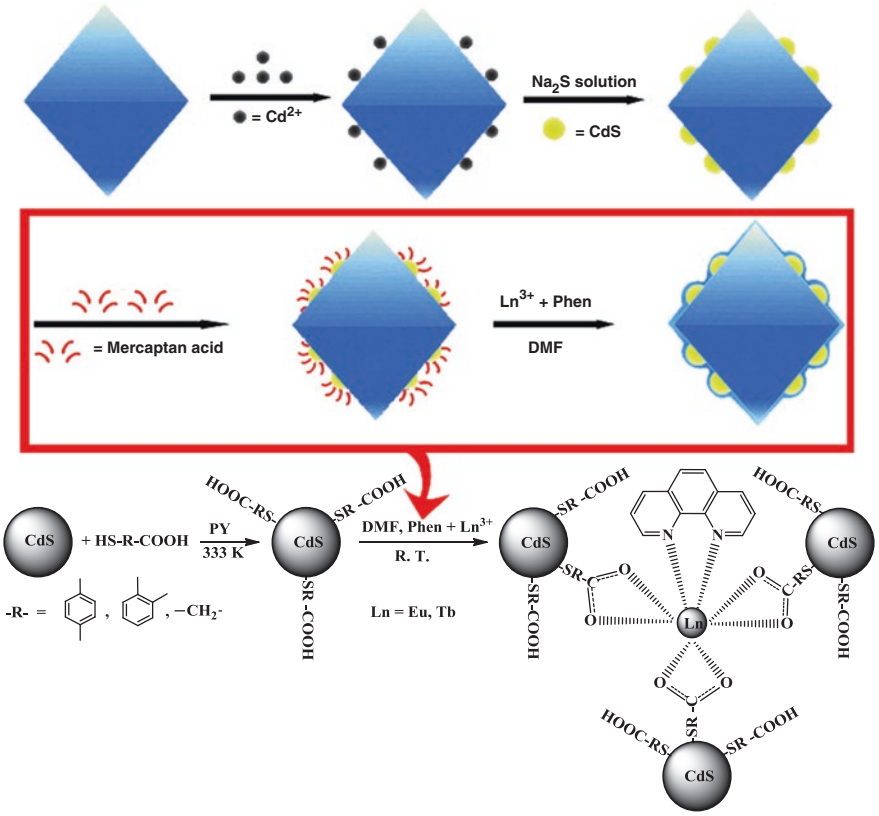

Fig. 4.6 The scheme for the synthesis procedure of rare earth complexes functionalized CdS-ZY and the predicted structure of the rare earth ternary complex functionalized CdS-ZY hybrid materials. Reprinted with permission from Ref. [19]. Copyright 2014 the Royal Society of Chemistry

The ratio of the intensities of the red and green emissions increases gradually with the increase of Eu^{3+} content (Figure 4.5B parts f–i). Furthermore, changes in the ratio of the three colored components as a function of the excitation wavelength and temperature are attained only by using zeolites as a host. The zeolite supercage incorporated with various amounts of three colored components provides an ideal environment to control the energy transfer processes that take place between them as a function of the excitation wavelength and temperature.

Recently, Duan et al. prepare a series of CdS-ZY hybrid materials via a mild coordination reaction (ZY = zeolite Y). The synthesis procedure and the predicted structure of the CdS-ZY hybrid material are shown in Fig. 4.6 [19]. In the first step, the synthesized zeolite Y crystal is loaded with Cd^{2+} ions through ion exchange process, and then an ethanol solution of sodium sulfide is used to react with cadmium ion-loaded zeolite, resulting in the CdS-zeolite Y hybrids. CdS QDs are proved by TEM images not only in the pores of zeolite but also on the surface of ZY

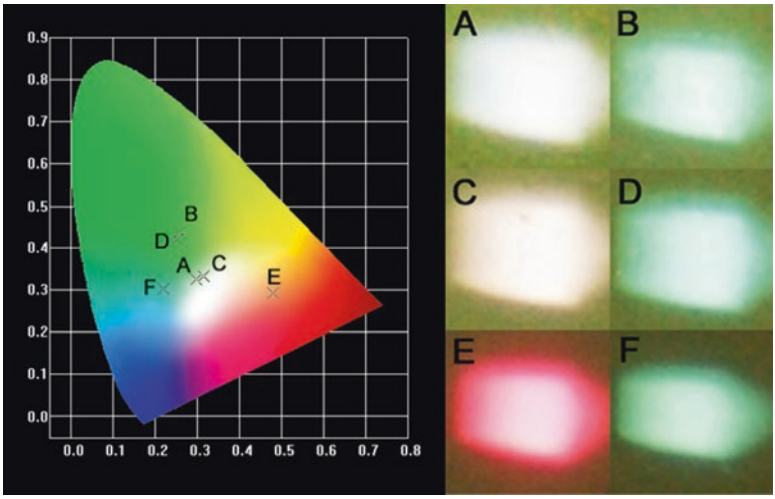

Fig. 4.7 CIE x-y chromaticity diagrams of hybrid materials. (*A*) Eu(phen)(*o*-MBA)$_3$-CdS-ZY (λ_{ex} = 296 nm) (*B*) Tb(phen)(*o*-MBA)$_3$-CdS-ZY (λ_{ex} = 297 nm) (*C*) Eu(phen)(*p*-MBA)$_3$-CdS-ZY (λ_{ex} = 321 nm) (*D*) Tb(phen)(*p*-MBA)$_3$-CdS-ZY (λ_{ex} = 323 nm) (*E*) Eu(phen)(MAA)$_3$-CdS-ZY (λ_{ex} = 298 nm) (*F*) Tb(phen)(MAA)$_3$-CdS-ZY (λ_{ex} = 298 nm) (Reprinted with permission from Ref. [19]. Copyright 2014 the Royal Society of Chemistry)

crystal. The aggregation of CdS QDs exists on the external surface of zeolite since a small amount of Cd^{2+} ions cling to the zeolite surface during introduction of S^{2-} ions. In the next step, three different mercaptan acids are performed separately on the CdS-ZY hybrids to modify CdS QDs, from which a coordination reaction is performed among mercaptan acid-modified CdS-ZY, phen, and rare earth ion.

The distribution of CdS QDs can be confirmed by the UV–vis diffusion reflection spectra. In the case of CdS QDs, the absorption maxima wavelength of the isolated QDs, interconnected QDs, and mesosized QDs appear in the 200 ~ 300 nm, 300 ~ 380 nm, and 380 ~ 480 nm regions, respectively. Therefore, it can be predicted from UV–vis reflection spectra that intrazeolite CdS QDs exist in zeolite Y crystals in three types, isolated, interconnected, and mesosized. Interestingly, the photoluminescence color can be tuned from white and pink to red by changing the coordination mercaptan acid. Figure 4.7 shows the corresponding CIE chromaticity diagram of europium or terbium complexes functionalized CdS-ZY with different coordination mercaptan acid. The corresponding luminescence color can be seen clearly from the photographs of europium or terbium complexes functionalized CdS-ZY samples, where an appropriate wavelength is used as the excitation source.

Sendor et al. load Eu^{3+} complexes of TTA to the supercages of zeolite X to improve the luminescence intensity of Eu^{3+}, in which lattice atoms participate in the luminescence mechanism via polar interaction and coordination [20]. But isolated complex within the large cavities of ZX structure may be observed, depending on composition and spatial consideration. The strong excitation band in near ultraviolet region is matchable to ultraviolet excited LED, enabling the potential applications of this material in sensors or lighting devices.

4.3 Photofunctional Rare Earth Hybrid Materials Based on Functionalized Zeolite A

Zeolite A (abbreviated as ZA) has a three-dimensional network of cavities, and the composition of its Na^+ form is $Na_{12}[(SiO_2)_{12}(AlO_2)_{12}]$. Yan's group first assemble the photofunctional rare earth hybrid materials through the functionalization of ZA host. Hao et al. prepare the host–guest assemblies of ZA and their thin films [21]. The assembly of zeolite A is done by first embedding rare earth complexes ($Eu(TTA)_n$ or $Tb(TAA)_n$) into the cages of ZA and then grafting another lanthanide complexes (Eu(L) or Tb(L), L = bpy or phen) onto the surface of functionalized ZA via 3-methacryloyloxypropyltrimethoxysilane (γ-MPS) (Fig. 4.8 (Top)). Firstly, the dependence of the crystal stability of ZA as the host of rare earth complexes on the level of ion exchange is studied by XRD, indicating that the degradation and partial collapse of ZA framework occur upon doping high amount of lanthanide complexes into its channels. While through properly controlling ion exchange extent, the integrity of ZA framework is well maintained after fabrication. Secondly, the obtained thin films of ZA assemblies are provided with the property of homogeneous dense packing and the high coverage degree of the crystals on the ITO glass, as displayed in SEM images (Fig. 4.8(Middle) c,d). The surface of the crystal becomes cruder, which may be caused by the follow-up surface modifications. Figure 4.8 (Middle) d reveals the homogeneous dense packing and the high coverage degree of the crystals on the ITO glass. The method to prepare the thin films of ZA assembly is by spin-coating via molecular linker, thus probably leading to the stronger interaction between the crystal base and the substrates, which is more conducive to make the crystals to stay on the glass tightly through chemical bonds. Thirdly, white light-emitting materials are obtained from a three-component system that comprises a blue-emitting ZA matrix, a red-emitting europium complex, and a green-emitting terbium complex. Various photoluminescence colors from the uniform thin films of ZA assembly can be fine-tuned both by purposely selecting the rare earth complexes inside and outside of ZA and by varying the excitation wavelength. Four red–green–blue (RGB) photoluminescence materials display white lights. Photographs of the photoluminescence colors from thin films are shown in Fig. 4.8 (Bottom).

Chen et al. introduce Eu/Tb complex and rare earth (Eu, Tb, Dy) polyoxometalates (REW_{10}) to functionalize ZA and titania through an inside–outside double modification path [22]. Eu/Tb complex-modified ZA (TTA-Eu(AA-Tb) ⊂ ZA) is achieved by ionic exchange reaction and gas dispersion. REW_{10}-modified titania (Ti-IM-REW_{10}) is obtained with the ionic liquid compound as the linker. Then multicomponent hybrids TTA-Eu(AA-Tb) ⊂ ZA-Ti-IM-REW_{10} are assembled through condensation reaction between hydroxyl groups on the surface of ZA and titania (Fig. 4.9 (top)). The selected SEM image of the cylindrical structure of these hybrids indicates that the crystal framework belonging to ZA still can be observed except that it becomes irregular as pure ZA due to the introduction of other functionalized components in the hybrid system. Figure 4.9 (Bottom) shows the selected digital photos of hybrid materials TTA-Eu ⊂ ZA-Ti-IM-EuW_{10} and AA-Tb ⊂ ZA-Al-IM-

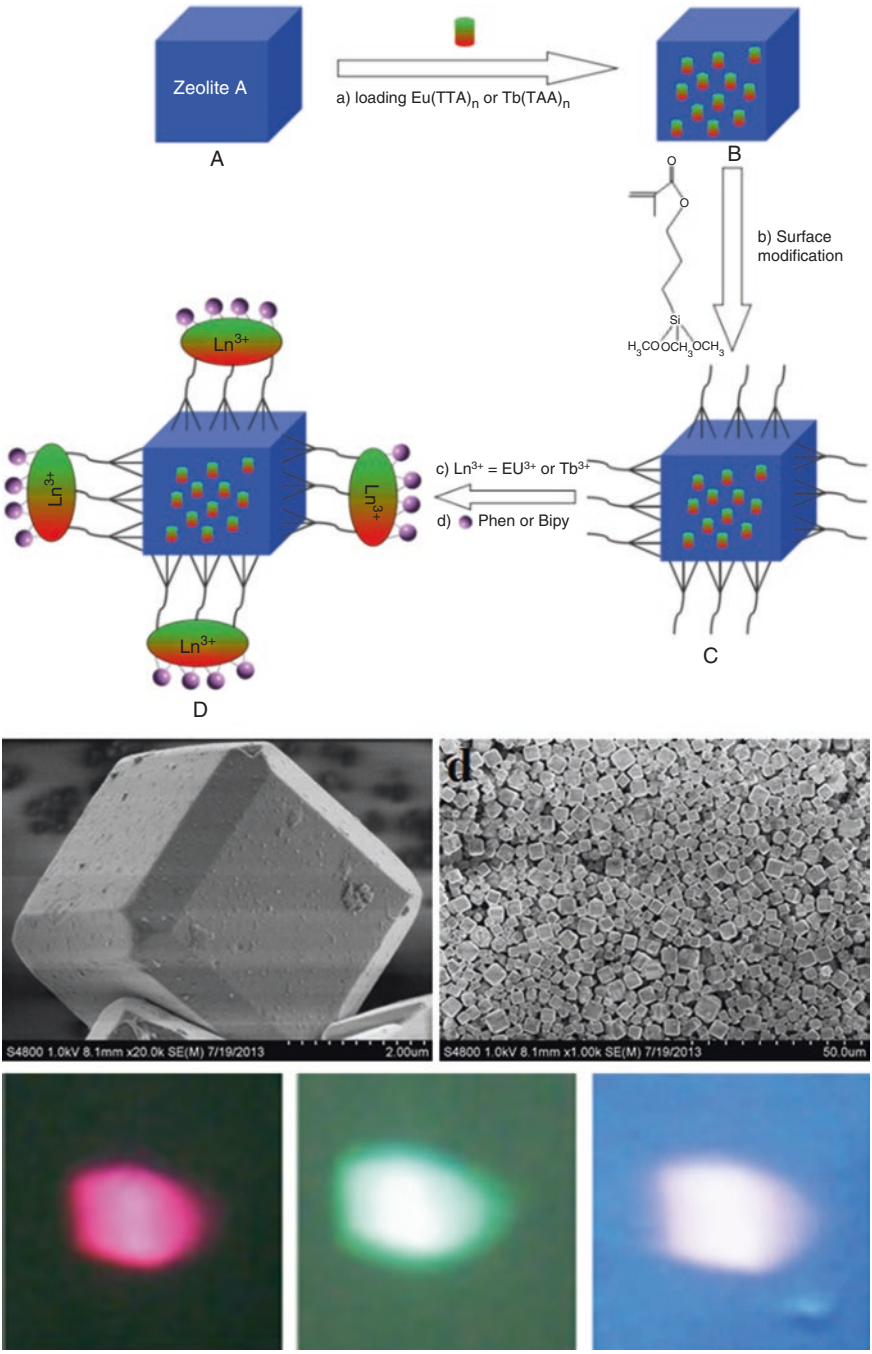

Fig. 4.8 (*Top*) The scheme for synthesis procedure and predicted structure of the hybrid materials of RE(L_2)-γ-MPS-[RE(L_1)$_n$-ZA]: (*a*) inserting lanthanide complexes into the cages of zeolite A; (*b*) fixing γ-MPS on the external surface of RE(L_1)$_n$-ZA through Si-O-Si; (*c*) further anchoring Ln^{3+} via C = O groups of γ-MPS; and (*d*) introducing phen or bpy ligands to coordinate with RE^{3+}.

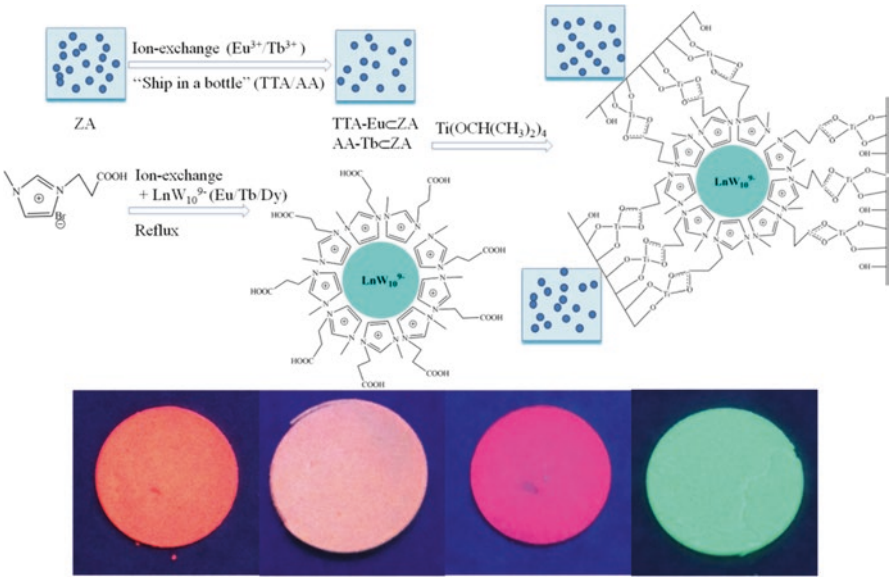

Fig. 4.9 (*Top*) The scheme for synthesis process and composition for the hybrid materials TTA-Eu(AA-Tb) ⊂ ZA-Ti-IM-LnW_{10} (Ln = Eu, Tb, Dy). (*Bottom*) The selected digital photos of hybrid materials TTA-Eu ⊂ ZA-Ti-IM-EuW_{10} (*left* two, λ_{ex} = 254 and 365 nm, respectively) and AA-Tb ⊂ ZA-Ti-IM-EuW_{10} (*right* two, λ_{ex} = 254 and 365 nm, respectively) under UV irradiation (Reprinted with permission from Ref. [22]. Copyright 2015, Springer)

EuW_{10} under UV irradiation of two wavelengths (254, 365 nm). For TTA-Eu ⊂ ZA-Ti-IM-EuW_{10} hybrids, the color of the hybrids changes from orange–red to violet–red for the different dominant europium luminescent species. More apparent for AA-Tb ⊂ ZA-Al-IM-EuW_{10} hybrids, its color changes from light purple–red to light blue–green. So the selective excitation of the hybrids can realize the color tuning for the two luminescent species.

Hao et al. prepare the PEMA-P4VP polymer thin films co-doped with the rare earth-ZA via coordination bond by a two-step procedure (Fig. 4.10 (Top)) [23]. Firstly, rare earth complexes are embedded into the cages of ZA, leading to RE-ZA host–guest materials with a marked enhancement of thermal stability or photostability as well as attractive luminescent properties. They choose two trialkoxysilyl derivatives of polydentate ligands as bridging molecules to graft the rare earth complexes which coordinate to the polymer chain on the external surface of rare earth-

Fig. 4.8 (continued) (Middle) SEM images of thin films of the final hybrid materials. (*Bottom*) The photographs of the photoluminescence colors from the thin films with the UV excitation using a Xe lamp as the excitation source: the images from left to right stand for Eu(L)-γ-MPS-[$Eu(TTA)_n$-ZA] (*red light*), Tb(L)-γ-MPS-[$Tb(TAA)_n$-ZA] (*green light*), and Tb(L)-γ-MPS-[$Eu(TTA)_n$-ZA] or Eu(L)-γ-MPS-[$Tb(TAA)_n$-ZA] (*white light*), respectively (Reprinted with permission from Ref. [21]. Copyright 2014 the Royal Society of Chemistry)

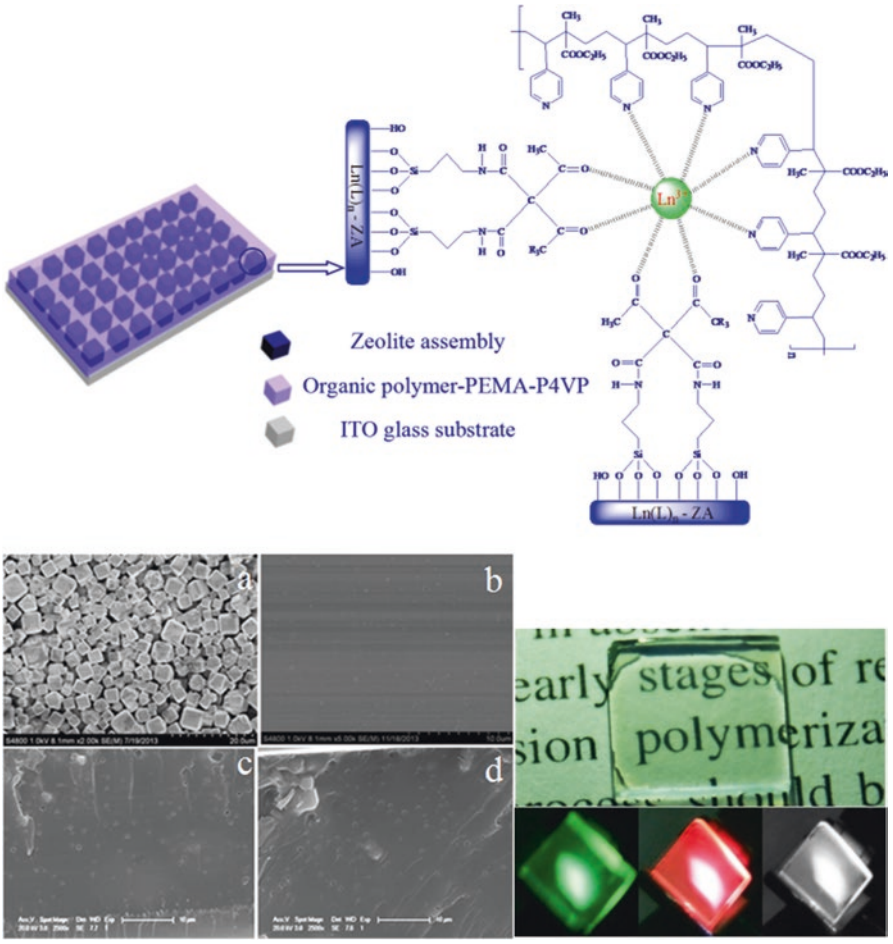

Fig. 4.10 (*Top*) The scheme for the synthesis procedure and predicted structure of the polymer thin films of PEMA-P4VP-RE-TAA-Si/AA-Si-[RE(L)-ZA]. (*Bottom*) SEM images of (*a*) ZA and a typical (*b*) surface and (*c*, *d*) cross-sectional SEM images of hybrid polymer thin film (*left*); and photographs of the transparent thin films and the photoluminescence colors from the organic polymer thin films with the UV excitation using a Xe lamp as the excitation source: *green* for terbium, *red* for europium, and *white* for Eu^{3+}/Tb^{3+} hybrids, respectively (*right*) (Reprinted with permission from [23]. Copyright 2014 the Royal Society of Chemistry Publishing Company)

doped ZA, thus dispersing RE-functionalized ZA into the organic polymer. The SEM image and the size distribution histogram in Fig. 4.10 (top, a) show that the ZA particles are monodispersed with an average particle size of 2.0 μm. Dispersion of the RE^{3+} complex-loaded ZA in the polymer matrix through chemical bond is investigated by surface and cross-sectional SEM (Fig. 4.10 (Bottom), left b, c, d). Several white spots in the images which are even distributed on the smooth background of the PEMA-P4VP polymer originate from zeolite A. And from the surface

and cross-sectional images, it can be further inferred that there exists a homogeneous dispersion of zeolite crystals throughout a polymer matrix. In this system, three kinds of photoluminescence colors are obtained, green, red, and white light from Eu^{3+} hybrids, Tb^{3+} hybrids, and Eu^{3+}/Tb^{3+} co-doped hybrids, respectively (Fig. 4.10 (Bottom), right). The bright white light is expected to have the potential and significant applications in optoelectronic devices in the future.

Chen et al. prepare some multicomponent hybrids based on zeolite L/A [24]. Firstly zeolite A/L is loaded with rare earth complexes (Eu-DBM or Tb-AA into their channels. Secondly, γ-MPS is used to covalently graft onto the surface of functionalized zeolite A/L (Si-[ZA/L ⊃ Eu-DBM(Tb-AA)]). Thirdly, rare earth ions (Eu^{3+}/Tb^{3+}) are coordinated to the functionalized zeolite A/L and ligands (phen or bipy). Some hybrids display white or near-white light emission. Further, above-selected hybrids are fabricated into PEMA/PMMA (poly ethyl methacrylate/polymethyl methacrylate) host to prepare luminescent polymer films. Chen et al. assemble a series of multicomponent photofunctional hybrid materials based on lanthanide polyoxometalates ($Na_9LnW_{10}O_{36}{\cdot}32H_2O$, LnW_{10}, Ln = Eu, Tb, Sm and Dy), ionic liquids (IMCl), and functionalized ZA/ZL through an inside–outside double modification path [25]. Here 1-methyl-3-(trimethoxysilylpropyl)imidazolium chloride (IM^+Cl^-) is covalently grafted onto the functionalized zeolite A/L and linked to lanthanide polyoxometalates as a double linker. These hybrids own two luminescence centers, one is rare earth complexes, and the other is lanthanide polyoxometalates. By adjusting the different components of the hybrids, the luminescent tuning and integration of various colors (white, warm white, green, and red light) can be realized.

4.4 Photofunctional Rare Earth Hybrid Materials Based on Functionalized Zeolite L

Zeolite L (ZL) crystals feature strictly parallel channels arranged in a hexagonal symmetry, and the particle size and aspect ratio of the colorless crystallites can be tuned over a wide range. The one-dimensional channels of ZL can be filled with suitable guests and geometrical constraints imposed by the host structure lead to supramolecular organization of the guests in the channels. Three main stages exist in the organization to form guest–host hybrid materials: supramolecular organization of dyes inside the ZL channels allowing light harvesting within the volume of a dye-loaded ZL crystal and radiationless energy transport to either the cylinder ends or to the center of the channel through one-dimensional excitation energy transport, the coupling of an external acceptor or donor stopcock fluorophore to the ends of the ZL channels to trap or inject electronic excitation energy, and interfacing the material to an external device through a stopcock intermediate. It is worth pointing out that Calzaferri's group has done the pioneering work on the functionalization of ZL-based hybrids for photophysical application [26].

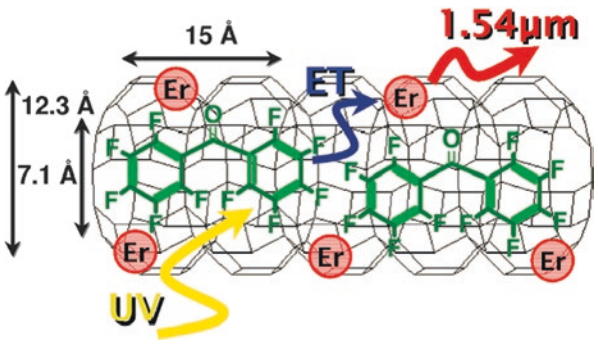

Fig. 4.11 Sketch showing the dimension of the ZL pore and schematic illustration of the energy transfer between dye and Er^{3+} inside the zeolite nanochannel (Reprinted with permission from Ref. [28]. Copyright 2010 the American Chemical Society)

For example, Monguzzi et al. use the ZL with highly crystalline microcrystals consisting of parallel arrays of nanometric channels to produce the desired confinement between the sensitizer and the emitting ion [27]. Ionic exchange of positive counterions with Er^{3+} and then benzophenone is introduced to form the final hybrid system. Subsequently, they obtain microcrystals suitable for NIR light emission by ion exchange of the zeolite charge-compensating cations (Na^{+}, Ca^{2+}) with Er^{3+} ions. Benzophenone is used as a light-harvesting molecule, which is a well-known triplet emitter for Er^{3+} sensitization. This approach has a number of potentially useful advantages. Inclusion of antenna molecules into the pores can provide an indirect excitation for the ion through a RET process. Optical pumping using LED or lamps rather than laser becomes feasible using this broadband sensitization. Through proper chemical functionalization, zeolites can be made compatible with polymer matrix to open the possibility of fabricating plastic photonic devices. The pump power required for population inversion in Er^{3+}-based optical amplifiers can then be lowered from more than 10^3 W/cm^2 to less than 1 W/cm^2, thus opening the way for important telecom applications.

Mech et al. demonstrate the possibility to obtain sensitized, highly efficient NIR emission of Er^{3+} ions exchanged within a ZL matrix [28]. The 1.5 μm emission is excited via energy transfer from loaded decafluorobenzophenone (DFB) molecules that upon filling the zeolite, nanochannels act as light-harvesting antenna (Fig. 4.11). Removal of water molecules from ZL structure and the use of perfluorinated organic molecules result in a strongly enhanced NIR emission (1.54 μm, $^4I_{13/2} \rightarrow {}^4I_{15/2}$ of Er^{3+}) with a longer lifetime (>2 orders of magnitude longer) than in erbium complexes with organic, nonfluorinated ligands. The full width at half maximum (fwhm) of the 1.54 μm PL band (~86 nm) is substantially broader than those observed for the Er^{3+} doped into inorganic hosts and most of the erbium (III) organic complexes, which is beneficial for wave division multiplexed signal amplifications. The intrinsic quantum yield of the sensitized luminescence is estimated to be 2.5%, which is one of the highest values reported for the 1.54 μm emission of Er^{3+} ions sensitized

by organic dyes. This approach may open a new way of manufacturing efficient NIR-emitting plastic-compatible devices useful in a broad spectrum of communication applications, because functionalized zeolites can be successfully incorporated into polymer matrices.

In recent years, on the basis of work of Calzaferri's group, Li's group has done an extensive and deep investigation on the functionalized ZL to assemble the photofunctional rare earth host–guest hybrid materials. Their research involves the control of morphology and size of ZL microcrystals, the assembly of rare earth complexes in the channel of ZL, the self-assembly of ZL induced by rare earth complexes, the ZL–polymer transparent hybrid materials, etc. [29]. For example, Wang et al. graft terbium complexes onto nanozeolite L material and prepare the hybrid material by first functionalizing ZL with (3-aminopropyl)triethoxysilane (APES) and then grafting carboxyphenyl isothiocyanate via the reaction of amino group covered on ZL surface and isothiocyanate groups. The functionalized ZL is at last reacted with Tb^{3+} ions [30]. They also realize the striking increase of Eu^{3+} and Tb^{3+} emission for the formation of $RE^{3+}(bpy)_n$ complexes (RE = Eu, Tb) inside the nanochannel of ZL upon gas-phase insertion of bpy into RE^{3+}-exchanged ZL crystals [31]. The new host–guest materials are suited to cooperate with UV-emitting LEDs because they can be excited in the near UV region. Furthermore, these materials can be tested for fabrication of different plastic photonic devices based on the recently published procedure of realizing transparent zeolite–polymer hybrid materials by means of a suitable functionalization of the external surfaces. Li et al. prepare luminescent rare earth complexes loaded ZL/silica core-shell hybrids and demonstrate the ability to further functionalize the core-shell hybrids for the luminescence sensing of dipicolinic acid (DPA), which is a major constituent of many pathogenic spore-forming bacteria [32]. This study also extends the application of ZL-based hybrid materials to the field of biosensors. Owing to the versatility of zeolite crystals and the luminescent dyes, the present approach should allow for the synthesis of novel core-shell hybrid materials for future sensing. The advantage of ZL compared to silica is that it can prevent the self-aggregation of dyes and superimpose a specific organization (the anisotropic intense luminescence with a high concentration of monomers).

Furthermore, Wang et al. achieve higher organization and additional functionality by a functional linker that has the ability to coordinate and sensitize lanthanide ions RE^{3+} and that is also able to self-assemble on a surface through hydrogen bonding (Fig. 4.12) [33]. They synthesize the triethoxysilylated molecule and test its ability to bind on a quartz substrate, to coordinate RE^{3+} ions and sensitize their luminescence. The flexible linker has two urea groups capable of forming hydrogen bridges. Substrate functionalized by the linker should then be able to form monolayers of oriented ZL microcrystals, resulting in the functionalized quartz plates, which can then be immersed in a suspension of ZL crystals to form the final hybrid monolayers. These hybrid materials present densely packed ZL monolayers, all of which stand on the substrate with their c axis perpendicular to the surface. This orientation and the high degree of coverage imply that the interaction between the crystal base and the substrate is much stronger than any other interactions.

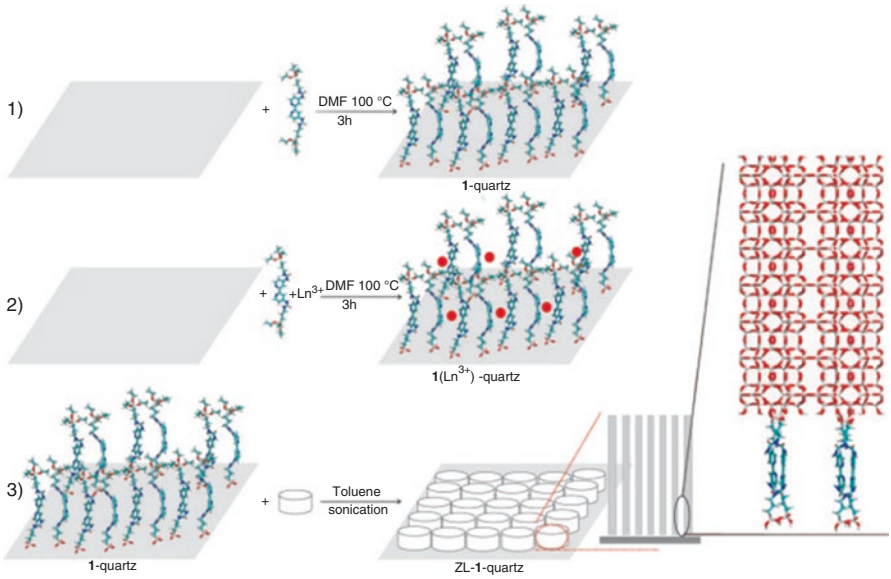

Fig. 4.12 Scheme for the bonding of ORMOSILs to the hydroxyl groups of a quartz substrate and subsequent formation of oriented open-channel monolayers (Reprinted with permission from Ref. [33]. Copyright 2010 Wiley)

Cao et al. further try the self-assembling ZL crystals into uniformly oriented layers with both the transition metal cations Zn^{2+}/Cu^{2+} and the lanthanide cations Eu^{3+}/Tb^{3+} that work effectively in binding and organizing the ZL crystals (Fig. 4.13) [34]. The cooperative interaction of terpy and metal cations is successful to assemble the uniformly oriented monolayer. Two different strategies, the S-L(M) and S-(L-M-L) methods, have been applied for lanthanide ions. The outlined principle is expected to be successful also for organizing other nano- or microsized objects bearing nanochannel. The self-assembly procedure is so versatile and robust that tailoring the properties of layers for meeting desired functionalities for a specific application is possible.

Ding et al. prepare photostable and efficient red-emitting host–guest hybrid materials employing a ship-in-bottle procedure by loading TTA or TTA and phen from gas phase into the channels of Eu^{3+}-ZL crystals that exhibit disk-shaped morphology followed by treatment with ammonia gas [35]. The emission intensity and the lifetime of Eu^{3+} ions of the host–guest materials can be significantly increased by treatment with ammonia gas, and the encapsulated Eu^{3+} complexes in ZL crystals show remarkably increased photostability; the insertion of organic ligand into the Eu^{3+}-ZL crystals leads to a striking increase in the emission intensity of Eu^{3+} ions as a result of the formation of Eu–TTA complexes. Furthermore, the significant increase in both the emission intensity and the decay times of Eu^{3+} ions by ammonia

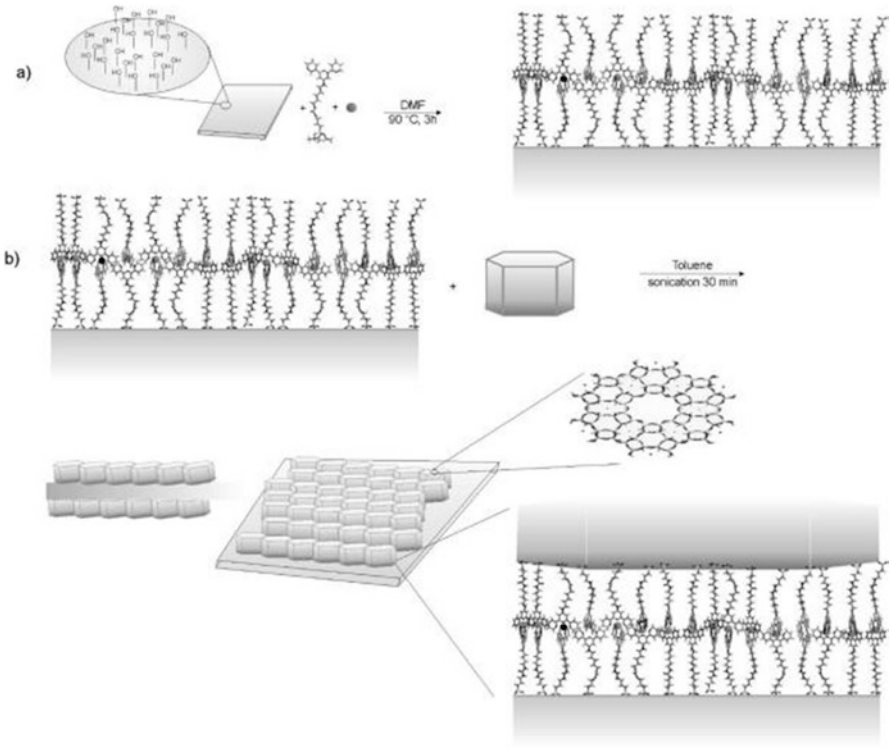

Fig. 4.13 S-(L-M-L) method for synthesizing ZL-L(M^{n+})L-S-L(M^{n+})L-ZL c-ocMLs. (*a*) The ligand is attached to the substrate in the presence of metal cations (indicated as *spheres*, e.g., Zn^{2+}, Cu^{2+}, or lanthanide Ln^{3+}), thus forming a L(M^{n+})L-S-L(M^{n+})L layer. (*b*) ZL crystals are attached to this layer. Conditions are such that they react preferentially with their base (Reprinted with permission from Ref. [34]. Copyright 2011 the American Chemical Society)

gas treatment may imply a potential use in ammonia sensing. Wen et al. investigate the acidity of Eu^{3+}-exchanged ZL and its influence on the luminescent performances of encapsulated Eu^{3+}–β-diketonate complexes [36]. The acidity of Eu^{3+}/ZL is determined roughly by using a dye (thionine) as the probe molecule. The luminescence behavior of the host–guest materials can be tuned by changing the acidity inside the channels of the zeolite L crystals and can potentially be used as a sensor for detecting ammonia.

Li et al. design a simple and robust platform to detect basic molecule vapors based on the encapsulation of Eu^{3+}–β-diketonate complexes within a nanozeolite L framework, which shows a condition selective luminescence turn-on response to basic molecule vapors [37]. The stationary and time-resolved spectroscopy studies suggest that the mechanism responsible for the turn-on response to basic molecule vapors is that basic molecules are favorable for the formation of Eu^{3+}–β-diketonate complexes with high coordination numbers by decreasing the proton strength of the channels. The turn-on luminescence response can be switched off by acidic vapors.

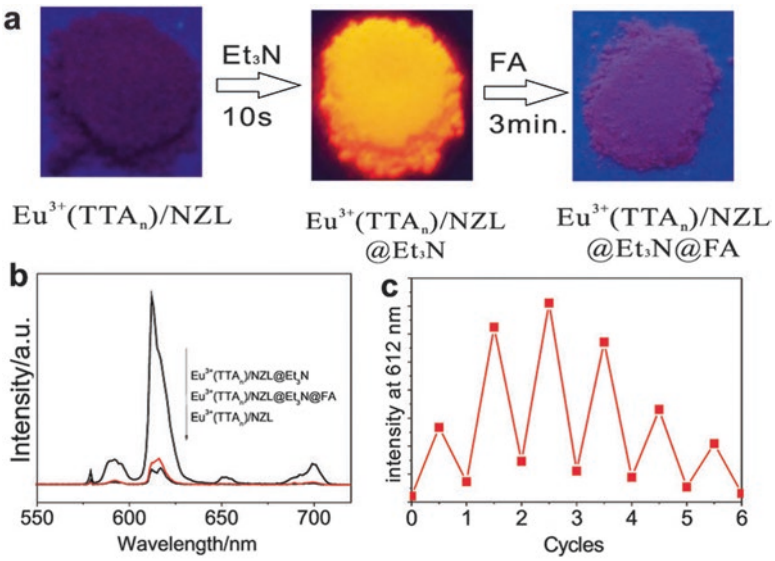

Fig. 4.14 Acid–base vapor-induced luminescence switching of $Eu^{3+}(TTA)_n$–NZL. (*a*) Digital photos of $Eu^{3+}(TTA)_n$–NZL during the exposure to Et_3N–FA vapor; (*b*) emission spectra of $Eu^{3+}(TTA)_n$–NZL showing spectral changes before and after exposure to Et_3N–FA vapor; (*c*) responses of emission intensity at 612 nm of $Eu^{3+}(TTA)_n$–NZL during the Et_3N–FA vapor exposure cycles (Reprinted with permission from Ref. [37]. Copyright 2012 the Royal Society of Chemistry)

Interestingly, when the used $Eu^{3+}(TTA)_n$–NZL samples are exposed to a formic acid (FA)–gas-enriched environment for several seconds, red luminescence disappears and is not visible to the naked eye, while upon subsequent exposure to Et_3N vapor for 5 sec, red luminescence can be seen by the naked eye (Fig. 4.14). The emission spectra of the $Eu^{3+}(TTA)_n$–NZL film are recorded upon alternate exposure to FA gas and Et_3N over at least six cycles in order to examine the reversibility. The high selectivity toward basic molecules, the fast response and good reversibility, and the outstanding robustness are another merit of this method.

Stopper molecules attached to nanozeolite L (NZL) boost the luminescence of confined Eu^{3+}–β-diketonate complexes (Fig. 4.15) [38]. The mechanism responsible has been elucidated by comparing two different diketonate ligands with different pKa values and two aromatic imines, bpy and phen, and by applying stationary and time-resolved spectroscopy. They have found that all of the data support the interpretation that the presence of stopper is favorable to the sustainable formation of Eu^{3+}–β-diketonate complexes with high coordination numbers by decreasing the proton strength inside of the channels of NZL, the main influence being exerted by the stoppers directly bound to the channel entrance. The strongly luminescent transparent films can be prepared using aqueous suspension.

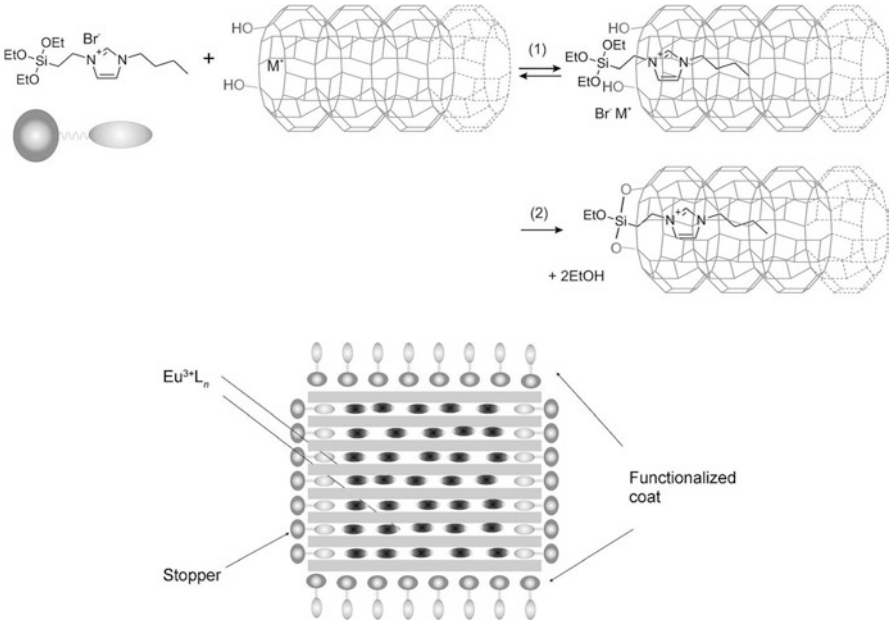

Fig. 4.15 *Upper*: selective modification of the ZL channel entrance; (*1*) sonication and (*2*) reflux. *Lower*: stopper- and coat-functionalized NZL crystal containing inside Eu^{3+} complexes as guests (Reprinted with permission from [38]. Copyright 2014 Wiley)

Li et al. obtain a luminescent and transparent hybrid material by embedding $Ln(L)_n$/ZL nanocrystals into a polymer (polymethyl methacrylate, PMMA) by means of a suitable functionalization of the external surface. In these hybrid materials, lanthanide complexes are encapsulated into the channels of nanosized ZL which are wrapped inside the polymers [39]. PMMA can prevent water molecules from quenching the luminescence of Eu^{3+}/Tb^{3+} inside the channels of nanosized ZL crystals. Functionalization of $Ln(L)_n$/ZL with methacryloxymethyltrimethoxysilane (MATMS) leads to $Ln(L)_n$/ZL-MATMS, and the transparent hybrids ($Ln(L)_n$/ZL-PMMA) are finally prepared from the radical polymerization of the monomer methyl methacrylate (MMA) and the $Ln(L)_n$/ZL-MATMS. Photographs show that the hybrid materials with a ZL content of 2 W/W% are highly transparent and show bright emission under UV illumination.

Liu et al. modify the photoluminescence properties of the $Eu(DBM)_3$ bath complexes by encapsulating it into the sub-nanometer pores of aluminosilicates zeolites L and Y [40]. The outer quantum efficiency of the Eu^{3+} emission and the photostability of Eu^{3+} are both improved considerably. Zeolite L is a more ideal host material for modification of lanthanide complexes. Besides, Chen et al. also functionalize ZL by some rare earth complexes of hydroxybenzene ketone derivatives [41, 42] and realize the multicomponent assembly of ZL with different rare earth luminescence species [43].

4.5 Conclusion and Outlook

In conclusion, recent research progress in the photofunctional rare earth materials based on nanoporous zeolite host has been summarized. The inside–outside double functionalization strategy and the self-assembly method have a special significance for zeolite-based photofunctional rare earth hybrid materials. It needs to mention that the crystal framework of zeolite is important for practical applications. The luminescent devices and sensors based on these hybrid materials should be developed extensively in the future.

References

1. Flanigen EM, Broach RW, Wilson ST (2010) Introduction, zeolites and molecular sieves. 1: zeolites in industrial separation and catalysis. Edited by Santi Kulprathipanja WILEY-VCH Verlag GmbH & co. KGaA, Weinheim
2. Breck DW (1974) Zeolite molecular sieves, structure, chemistry and use. Wiley, New York; Reprinted by Krieger, Malabar, Florida, 1984
3. Flanigen EM (2001) Zeolites and molecular sieves. An historical perspective, in Introduction to zeolite science and practice, 2nd edn (eds H. Van Bekkum, E.M. Flanigen, Jacobs PA, Jensen JC). Stud Surf Sci Catal 137:11–35
4. Devaux A, Minkowski C, Calzaferri G (2004) Electronic and vibrational properties of fluorenone in the channels of zeolite L. Chem Eur J 10:2391–2408
5. Baugis GL, Brito HF, de Oliveira W, de Castro FR, Sousa-Aguiar EF (2001) The luminescent behavior of the steamed EuY zeolite incorporated with vanadium and rare earth passivators. Microp Mesop Mater 49:179–187
6. Nakamura Y, Hasaegawa M, Katsuki K (2005) Microenvironments in faujasite-type Fe-al zeolites probed by europium luminescence. Chem Lett 34:490–491
7. Abry S, Lux F, Albela B, Artigas-Miquel A, Nicolas S, Jarry B, Perriat P, Lemercier G, Bonneviot L (2009) Europium(III) complex probing distribution of functions grafted using molecular stencil patterning in 2D hexagonal mesostructured porous silica. Chem Mater 21:2349–2359
8. Chen SH, Chao KJ, Lee TY (1990) Lanthanum-NaY zeolite ion exchange. 1. Thermodynamics and thermochemistry. Ind Eng Chem Res 29:2020–2023
9. Lee TY, TS L, Chen SH, Chao KJ (1990) Lanthanum-NaY zeolite ion exchange. 2. Kinetics. Ind Eng Chem Res 29:2024–2027
10. Atienzar P, Corma A, Garcia H, Serra JM (2004) High-throughput characterisation of materials by photoluminescence spectroscopy. Chem Eur J 10:6043–6047
11. Chen W, Sammynaiken R, Huang Y (2000) Photoluminescence and photostimulated luminescence of Tb^{3+} and Eu^{3+} in zeolite-Y. J Appl Phys 88:1424–1431
12. Justel T, Wiechert DU, Lau C, Sendor D, Kynast U (2001) Optically functional zeolites: evaluation of UV and VUV stimulated photoluminescence properties of Ce^{3+}- and Tb^{3+}-doped zeolite X. Adv Funct Mater 11:105–110
13. Mech A, Monguzzi A, Cucinotta F, Meinardi F, Mezyk J, De Cola L, Tubino R (2011) White light excitation of the near infrared Er^{3+} emission in exchanged zeolite sensitised by oxygen vacancies. Phys Chem Chem Phys 13:5605–5608
14. Li HR, Ding YX, Wang Y (2012) Photoluminescence properties of Eu^{3+}-exchanged zeolite L crystals annealed at 700 °C. CrystEngComm 14:4767–4771

15. Zhang HH, Li HR (2011) Efficient visible and near-infrared photoluminescence from lanthanide and bismuth functionalized zeolite L. J Mater Chem 21:13576–13580
16. Duan TW, Yan B (2014) Photophysical properties of metal ion functionalized NaY zeolite. Photochem Photobiol 90:503–510
17. Wada Y, Okubo T, Ryo M, Nakazawa T, Hasegawa Y, Yanagida S (2000) High efficiency near-IR emission of Nd(III) based on low-vibrational environment in cages of nanosized zeolites. J Am Chem Soc 122:8583–8584
18. Wada Y, Sato M, Tsukahara Y (2006) Fine control of red–green–blue photoluminescence in zeolites incorporated with rare-earth ions and a photosensitizer. Angew Chem Int Ed 45:1925–1928
19. Duan TW, Yan B (2014) Novel luminescent hybrids by incorporating a rare earth ternary complex into CdS QDs loaded zeolite Y crystals through coordination reaction. CrystEngComm 16:3395–3402
20. Sendor D, Kynast U (2002) Efficient red-emitting hybrid materials based on zeolites. Adv Mater 14:1570–1574
21. Hao JN, Yan B (2014) Photofunctional host-guest hybrid materials and thin film of lanthanide complexes covalently linked to functionalized zeolite a. Dalton Trans 43:2810–2818
22. Chen L, Yan B (2015) Photofunctional hybrid materials with polyoxometalates and benzoate modified mesoporous silica through double functional imidazolium ionic liquid linkage. Coll Polym Sci 293:1847–1853
23. Hao JN, Yan B (2014) Hybrid polymer thin films with a lanthanide-zeolite a host-guest system: coordination bonding assembly and photo-integration. New J Chem 38:3540–3547
24. Chen L, Yan B (2015) Multi-component lanthanide hybrids based on zeolite a/L and zeolite a/L-polymer for tunable luminescence. Photochem Photobiol Sci 14:358–365
25. Chen L, Yan B (2015) Multi-component assembly and luminescence tuning of lanthanide hybrids through the inside-outside double modification of zeolite A/L. New J Chem 39:4154–4161
26. Calzaferri G, Huber S, Maas H (2002) Host–guest antenna materials. Angew Chem Int Ed 42:3732–3758
27. Monguzzi A, Macchi G, Meinardi F, Tubino R, Calzaferri G (2008) Sensitized near infrared emission from lanthanide-exchanged zeolites. Appl Phys Lett 92:123301
28. Mech A, Monguzzi A, Meinardi F, Mezyk J, Macchi G, Tubino R (2010) Sensitized NIR erbium(III) emission in confined geometries: a new strategy for light emitters in telecom applications. J Am Chem Soc 132:4574–4576
29. Li HR, Wang Y, Cao PP, Ding YX, Zhang HH, Hu XJ, Wen TT (2012) Recent progress in host–guest luminescent functional materials based on lanthanide/zeolite L. Sci Chin-Chem (in Chinese) 42:1–18
30. Wang YG, Li HR, Zhang WJ, Liu BY (2008) Luminescence properties of nanozeolite L grafted with terbium organic complex. Mater Lett 62:3167–3170
31. Wang YG, Li HR, LJ G, Gan QY, Li YN, Calzaferri G (2009) Thermally stable luminescent lanthanide complexes in zeolite L. Microp Mesop Mater 121:1–6
32. Li HR, Cheng WJ, Wang Y, Liu BY, Zhang WJ, Zhang HJ (2010) Surface modification and functionalization of microporous hybrid material for luminescence sensing. Chem Eur J 16:2125–2130
33. Wang Y, Li HR, Feng Y, Zhang HJ, Calzaferri G, Ren TZ (2010) Orienting zeolite L microcrystals with a functional linker. Angew Chem Int Ed 49:1434–1438
34. Cao PP, Li HR, Zhang PM, Calzaferri GA (2011) Self-assembling zeolite crystals into uniformly oriented layers. Langmuir 27:12614–12620
35. Ding YX, Wang YG, Li HR, Duan ZY, Zhang HH, Zheng YX (2011) Photostable and efficient red-emitters based on zeolite L crystals. J Mater Chem 21:14755–14759
36. Wen TT, Zhang WJ, Hu XJ, He L, Li HR (2013) Insight into the luminescence behavior of europium(III) β-diketonate complexes encapsulated in zeolite L crystals. ChemPlusChem 78:438–442

37. Li HR, Zhang HH, Wang LY, Mu D, Qi ST, Hu XJ, Zhang L, Yu JS (2012) Highly luminescent Eu^{3+}-exchanged zeolite L crystals resulting from modification with silylated β-diketone. J Mater Chem 22:9338–9342
38. Li P, Wang YG, Li HR, Calzaferri G (2014) Luminescence enhancement after adding stoppers to europium(III) nanozeolite L. Angew Chem Int Ed 53:2904–2909
39. Li HR, Ding YX, Cao PP, Liu HH, Zheng YX (2012) Preparation and luminescence of transparent zeolite L-polymer hybrid materials. J Mater Chem 22:4056–4059
40. Liu HH, Song HW, Li SW, Ren XG, Lv SZ, Yu HQ, Pan GH, Zhang H, Hu LY, Dai QL, Qin RF, Yu JH, Wang GM, Jiang JX (2008) Preparation, characterization and photoluminescence properties of ternary europium complexes $Eu(DBM)_3$bath encapsulated into aluminosilicate zeolites. J Nanosci Nanotechnol 8:3959–3966
41. Chen L, Yan B (2014) Novel cool-white luminescent hybrids through host-guest assembly of 6-hydroxybenz[de]anthracen-7-one and europium ion exchanged zeolite L. Inorg Chem Comm 43:75–77
42. Chen L, Yan B (2014) Luminescent hybrid materials based on zeolite L crystals and lanthanide complexes: host-guest assembly and ultraviolet-visible excitation. Spectrochim Acta A 131:1–8
43. Chen L, Yan B (2015) Novel multi-component hybrids through of double luminescent lanthanide unit functionalized zeolite L and titania. Spectrochim Acta A 151:1001–1003